



Climate induced sub-basin source-area shifts of Zambezi River sediments over the past 17 ka



Janna Just ^{a,*}, Enno Schefuß ^a, Holger Kuhlmann ^a, Jan-Berend W. Stuut ^{a,b}, Jürgen Pätzold ^a

^a MARUM, Center for Marine Environmental Sciences and Faculty of Geosciences, University of Bremen, PO Box 330 440, D-28334 Bremen, Germany

^b Royal Netherlands Institute for Sea Research (NIOZ), PO Box 59, 1790 AB Den Burg, Texel, The Netherlands

ARTICLE INFO

Article history:

Received 16 January 2014

Received in revised form 19 May 2014

Accepted 31 May 2014

Available online 9 June 2014

Keywords:

Southeast Africa

Paleoclimate

Terrigenous sediments

Provenance

Heinrich Stadial 1

Holocene

ABSTRACT

Geochemical and mineralogical proxies for paleoenvironmental conditions have the underlying assumption that climate variations have an impact on terrestrial weathering conditions. Varying properties of terrigenous sediments deposited at sea are therefore often interpreted in terms of paleoenvironmental change. Also in gravity core GeoB9307-3 (18° 33.99' S, 37° 22.89' E), located off the Zambezi River, environmental changes during Heinrich Stadial 1 (HS 1) and the Younger Dryas (YD) are accompanied by changing properties of the terrigenous sediment fraction. Our study focuses on the relationship of variability in the hydrological system and changes in the magnetic properties, major element geochemistry and granulometry of the sediments. We propose that changes in bulk sedimentary properties concur with environmental change, although not as a direct response of climate driven pedogenic processes. Spatial varying rainfall intensities on a sub-basin scale modify sediment export from different parts of the Zambezi River basin. During humid phases, such as HS 1 and the YD, sediment was mainly exported from the coastal areas, while during more arid phases sediments mirror the hinterland soil and lithological properties and are likely derived from the northern Shire sub-basin. We propose that a de-coupling of sedimentological and organic signals with variable discharge and erosional activity can occur.

© 2014 Elsevier B.V. All rights reserved.

1. Introduction

Terrigenous materials exported by rivers and winds to the oceans are used to reconstruct past terrestrial environmental conditions. Elemental ratios measured on marine terrigenous materials are used as a proxy for weathering intensity and pedogenesis, since different elements are more mobile and will become depleted during intense chemical weathering (Boyle, 1983; Schneider et al., 1997; Zabel et al., 2001; Mulitza et al., 2008; Govin et al., 2012). The composition of pedogenically formed clay minerals depends on the geochemistry of the parent material and on soil humidity and temperature (Singer, 1980, 1984). Depending on the stability of individual minerals, clays may further be altered if environmental parameters change (Singer, 1980, 1984). Under this assumption marine records of clay mineralogy are used to trace sediments to source areas subject to differing climatic conditions (Biscaye, 1965; Caquineau et al., 2002; Meyer et al., 2013). The magnetic mineral content, e.g., the magnetic susceptibility, is often used to reconstruct changing terrigenous input (e.g. Bloemendal et al., 1992; deMenocal

et al., 2001). The magnetic mineralogy in igneous rock depends on the chemistry of the magmatic intrusion and cooling history (Clark and Emerson, 1991). Therefore magnetic properties can be used for provenance reconstructions (e.g., Oldfield et al., 1979; Maher et al., 2009; Mathias et al., in press). Furthermore, the primary magnetic mineralogy is overprinted during pedogenesis, whereby the dissolution or formation of magnetic minerals depends on soil moisture, Eh–pH conditions and temperature (Fitzpatrick and Schwertmann, 1982; Kämpf and Schwertmann, 1983; Maher and Taylor, 1988; Schwertmann and Taylor, 1989). Therefore the pedogenic magnetic mineral fabric can be used to reconstruct environmental changes during soil formation (Maher, 1986; Maher and Thompson, 1992) or to disentangle sediments derived from settings subject to differing weathering regimes (Schmidt et al., 1999; Heslop et al., 2007; Köhler et al., 2008; Larrasoña et al., 2008; Lyons et al., 2010, 2012; Just et al., 2012a) and soil types (Hanesch and Scholger, 2005).

In large river basins host rocks and soils may vary spatially. If sediments from specific parts of the catchment are delivered in varying contributions, this mixed signal can be recorded in the properties of the offshore deposited fluvial material. Studies focusing on this effect have been carried out on different timescales. Meade (1994) showed seasonally varying sediment contributions from different tributaries of the Amazon River. Similarly, the contributions from the White and Blue Nile vary seasonally (Williams et al., 2006 and references therein).

* Corresponding author at: University of Cologne, Institute of Geology and Mineralogy, Zùlpicher Str. 49a, Cologne, Germany.

E-mail addresses: janna.just@uni-koeln.de (J. Just), eschefuss@marum.de (E. Schefuß), kuhlma@marum.de (H. Kuhlmann), Jan-Berend.Stuut@nioz.nl (J.-B.W. Stuut), jpaetzold@marum.de (J. Pätzold).

Also on millennial time-scales the proportion of Blue and White Nile sediments varied in marine records, related to orbitally modified seasonality and rainfall (Blanchet et al., 2013).

The use of environmental proxies is complicated if sediment properties are biased during transport such as by gravitational fractionation (Caquineau et al., 2002; Bloemsmas et al., 2012). A careful consideration of all influencing factors is therefore crucial when using marine proxy records for environmental reconstructions.

Our study aims to elucidate if terrigenous proxies signify climate variations in the Zambezi Basin, are due to changing sediment provenance or result from grain-size fractionation during sediment transport.

We selected a gravity core off the Zambezi River (Fig. 1), SE Africa, located south of the modern Inter Tropical Convergence Zone's (ITCZ) austral summer position. It was previously shown that sediments in GeoB9307-3 (18° 33.99' S, 37° 22.89' E) record short-term climate perturbations during the past 17 ka (Schefuß et al., 2011). The core location receives terrigenous material exported by the Zambezi River which drains multiple sub-basins with differing basement lithologies, soils and vegetation assemblages. It was hypothesized that inverse relationships of vegetation changes and precipitation were due to shifts in the main source areas of terrestrial organic material delivered by the Zambezi River (Schefuß et al., 2011). Also a study focusing on the heavy-mineral assemblage on the shelf inferred that different facies represent material exported from the crystalline hinterland of Paleozoic age and from the coastal Pleistocene "Cover Sands", respectively (Beiersdorf et al., 1980). Because of the geographic and climatic setting as well as the lithological and pedogenic conditions in the Zambezi basin, our study site is well suited to test how climate change and sub-basin source-area changes are recorded in marine sediments.

We analyzed grain-size distributions of the land-derived sediment fraction, major element compositions and the magnetic mineral

inventories of gravity core GeoB9307-3 to evaluate effects of environmental change, gravitational fractionation and source area changes on sedimentary material delivered by the Zambezi River. Isothermal Remanent Magnetization (IRM) acquisition curves, that mirror the magnetic mineral inventory, have been used for end-member unmixing (Heslop and Dillon, 2007; Just et al., 2012a) to quantify sedimentary fractions derived from different parts of the basin.

2. Setting

The Zambezi River is 2500 km long and originates in northern Zambia, flows through eastern Angola and follows the border between Zambia and Zimbabwe through Mozambique to the Indian Ocean (Fig. 1). The catchment is with 1.385 million km² the 4th largest river basin in Africa and integrates over sub-catchments of various tributaries. Of these sub-catchments the highest water input is derived from the Upper Zambezi catchment (NW), the Luangwa (N) and Shire Rivers (E) (Zambezi Watercourse Commission, 2008). The coastal Shire contributes at present about 28% of the solid sediment load of the Zambezi. Before the construction of the Cahora Bassa dam (for location see Fig. 1) in the late 1960s, modeled sedimentary input by the Shire was around 21% (Ronco et al., 2006). The rainy season is in austral summer, when the ITCZ is located at its southernmost position. Annual precipitation in the Zambezi basin varies spatially with 1500 mm in the northern part, while the southern and central areas receive 850 mm and 600–700 mm, respectively (Ronco et al., 2006).

Most of the Zambezi Basin is composed of igneous and metamorphic rocks that are overlain by siliciclastic sediments in the river channel and coastal plain. Mineralogical analyses of the coastal so-called *Cover Sands* indicate a lower heavy-mineral content compared to modern

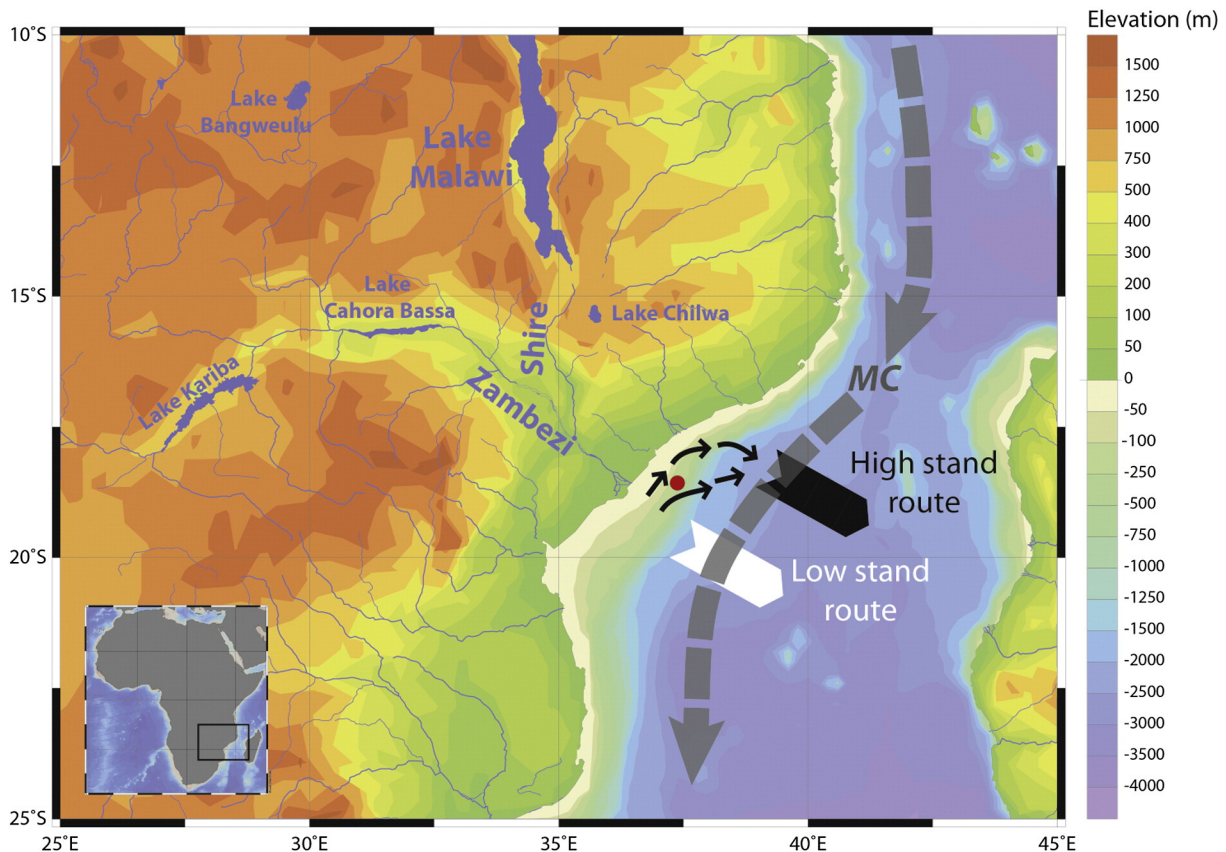


Fig. 1. Topographic map of the study area with site GeoB9307 (red point). The sediment export routes related to sea-level variations (after Schulz et al., 2011) are indicated by black and white arrows. MC: Mozambique Current.

suspended sediment load, the latter being related to the fresher soils developing on igneous rocks (Beiersdorf et al., 1980).

At present the fluvial material is captured by a northeastward flowing coast-parallel current on the shelf and is feeding the submarine Zambezi Valley (Schulz et al., 2011). In contrast, during the last glacial downslope sediment transport occurred through the Zambezi paleo-channel located off the River mouth (Beiersdorf et al., 1980; Schulz et al., 2011) (Fig. 1).

3. Materials and methods

Gravity core Geob9307-3 was retrieved during Meteor Cruise M63/1 in 2005 (Türkay and Pätzold, 2009) in a water depth of 542 m (Fig. 1). The 651 cm long sediment archive consists of hemipelagic green to brown mud and is composed of mixed contributions of marine biogenic and lithogenic material (Schefuß et al., 2011). The age model was constructed by linear interpolation between 19 radiocarbon dates obtained from mixed planktonic foraminifera shells (Schefuß et al., 2011) yielding a maximum age of 17 kyrs. Sedimentation rates strongly vary between 10 and 300 cm/kyr (Fig. 2) depending on fluvial discharge, which is mainly controlled by increases in precipitation during Heinrich Stadial 1 (HS 1; 15–18 ka) and the Younger Dryas (YD; 11.6–12.8 ka) (Schefuß et al., 2011). Furthermore, sedimentation rates are modulated by the location of sediment export routes and depocenters (Schulz et al., 2011, cf. Fig. 1).

3.1. XRF scanning

XRF Core Scanner data were collected every 1 cm over a 1.2 cm² area with a downcore slit size of 1 mm, using generator settings of 50 kV, a current of 1.0 mA for heavy elements and 10 kV, and 0.2 mA for light elements. Sampling time for both runs was 20 s. The measurements were conducted directly at the split core surface of the archive half with XRF Core Scanner II (AVAATECH Serial No. 2) at MARUM, University of Bremen. The core surface was covered with a 4 µm thin SPEXCerti Prep Ultralene1 foil to avoid contamination of the measurement unit and desiccation of the sediment. The here reported data have been acquired by a Canberra X-PIPS Silicon Drift Detector (SDD; Model SXD 15C-150-500) with 150 eV X-ray resolution, the Canberra Digital Spectrum Analyzer DAS 1000, and an Oxford Instruments 50 W XTF5011 X-ray tube with rhodium (Rh) target material. Raw data spectra were processed by the analysis of X-ray spectra by iterative least square software (WIN AXIL) package from Canberra Eurisys.

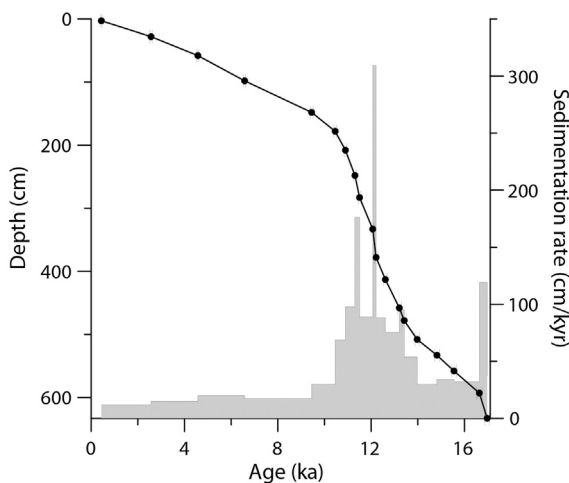


Fig. 2. Age-depth model and sedimentation rates (gray step plot) for gravity core Geob9307-3 (Schefuß et al., 2011). The age model was obtained by linear interpolation between radiocarbon dates (dots and error bars).

To calibrate the element intensities to concentrations, we collected 30 freeze-dried and homogenized discrete samples (5 g) for performing energy dispersive polarization X-ray Fluorescence (EDP-XRF) spectroscopy using a SPECTRO XEPOS instrument (Wien et al., 2005). For the calibration procedure transforming element intensities to relative concentrations of Fe, K, Ti, Zr, Si, and Al the log-ratio approach of Weltje and Tjallingii (2008) was applied with Ca as a common denominator.

3.2. Rock-magnetic measurements

Rock magnetic properties were measured on 6.2 cm³ samples taken at 5 cm spacings (~130 samples). Laboratory-induced remanence parameters were measured using an automated 2-G Enterprises 755R DC superconducting magnetometer. Anhysteretic Remanent Magnetization (ARM_{100 mT}) was induced with a 100 mT AF and a 40 µT DC bias field. ARM_{100 mT} indicates the presence of fine-grained single domain (SD) magnetite (King et al., 1982; Frederichs et al., 1999). Acquisition curves of IRM were obtained using an in-line pulse magnetizer (fields up to 0.7 T) and an “external” pulse magnetizer (up to 2.7 T, 2-G Enterprises). The IRM curves of each sample depend on the magnetic inventory because magnetic minerals have specific coercivities and thus IRM curves (e.g., Eyre, 1996; Frank and Nowaczyk, 2008). The magnetic remanence acquired at 100 mT (IRM_{100 mT}) represents the multidomain (MD) magnetite content (Frederichs et al., 1999). The forward S-Ratio $S = \text{IRM}_{300 \text{ mT}} / \text{SIRM}$ (Bloemendal et al., 1992; Kruiver and Passier, 2001) was used to estimate the ratio of low (e.g., magnetite) to high coercivity (hematite and goethite) minerals.

3.3. Grain-size distribution

To investigate grain-size fractionation processes, 71 discrete samples were analyzed in 10 cm increments, except 113–183 cm and 303–313 cm where sampling resolution was 5 cm. To obtain the grain-size distributions of the terrigenous sedimentary fraction, organic matter was removed by boiling 0.5 g of bulk sediment with H₂O₂ (35%) and afterwards with HCl (10%) and demineralized water to remove organics and CaCO₃. Particle sizes were measured using a Beckman Coulter laser particle sizer LS200 in 92 logarithmically-spaced size classes ranging from 0.39 to 2000 µm. Particles coarser than 300 µm were not observed.

3.4. End-member analyses

To obtain the mixing coefficients of terrigenous material derived from different source areas, we performed end-member (EM) unmixing on IRM acquisition curves, using the algorithm of Heslop and Dillon (2007) that adopts the approach of Weltje (1997).

The linear mixing system can be written in matrix notation as:

$$\mathbf{X} = \mathbf{AS} + \mathbf{R} = \hat{\mathbf{X}} + \mathbf{R}.$$

\mathbf{X} represents a n -by- m matrix of n samples and m IRM acquisition steps. \mathbf{A} (n -by- l) denotes the mixing coefficients of l EMs for the n samples. The m EM properties, representing the IRM acquisition curves of the l EMs, are contained in matrix \mathbf{S} (l -by- m). \mathbf{R} (n -by- m) denotes the residual matrix and $\hat{\mathbf{X}}$ represents the estimates of the mixing system.

4. Results

4.1. Downcore records

Fig. 3 shows selected parameters characterizing the sedimentary fraction. A sea-level reconstruction from the Indian Ocean (Camoin et al., 2004) is shown for comparison (Fig. 3a). Fe/Ca (Fig. 3c) is indicative of the ratio between terrigenous and marine materials. Elemental ratios such as Zr/(Si + Al + Fe + K + Ti) (further referred to as Zr/terr,

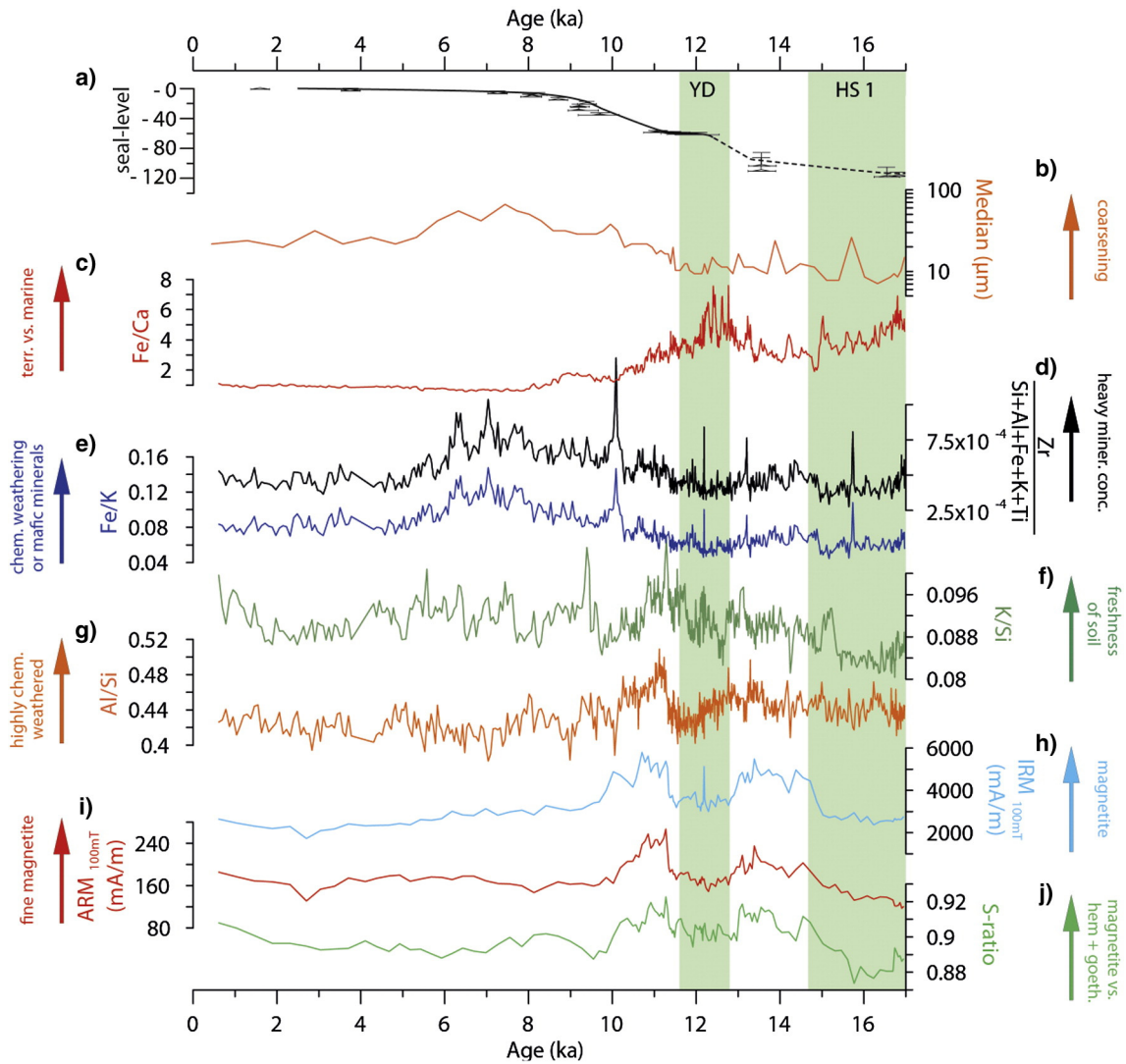


Fig. 3. (a) black line: composite sea-level curve for the Western Indian Ocean after Camoin et al. (2004). (b) median grain-size of the terrigenous fraction. (c–f) EDP-XRF calibrated elemental ratios: (c) Fe/Ca (Schefuß et al., 2011), (d) Zr/(Si + Al + Fe + K + Ti) in text referred to as Zr/terr, (e) Fe/K, (f) K/Si, and (g) Al/Si. (h–j) magnetic properties: (h) IRM_{100 mT}, (i) ARM_{100 mT}, and (j) S-Ratio.

Fig. 3d), Fe/K (Fig. 3e), K/Si (Fig. 3f) and Al/Si (Fig. 3g) depend on the composition of the terrigenous material, which is influenced by 1.) the source rock of the sediments, 2.) weathering processes and 3.) sediment-transport processes. These factors likewise control the concentration of magnetic minerals (IRM_{100 mT}, ARM_{100 mT}, Fig. 3h, i) and magnetite/(hematite + goethite) ratio (S-Ratio, Fig. 3j).

The median grain size is relatively constant in the lower part of the core (Fig. 3b). After 11 ka a coarsening trend is visible with a successive fining starting after ~7 ka. In contrast, variations are apparent in the concentration-dependent and compositional parameters in the lower part of the record. HS 1 is characterized by a high Fe/Ca and low K/Si and relative low Zr/terr and Fe/K ratios (Fig. 3c–f). The concentration of magnetic minerals is significantly lower (IRM_{100 mT}, Fig. 3h) and the proportion of goethite and hematite increases with respect to magnetite (S-Ratio, Fig. 3j). After HS 1, magnetic mineral concentration and K/Si increase, while Fe/Ca decreases. During the YD the magnetic mineral concentration and K/Si drop sharply while Al/Si, Zr/terr and Fe/K decrease more gradually (Fig. 3d–g). At the same time Fe/Ca shows a dramatic increase (Fig. 3c). Successively, the magnetic parameters and Al/Si and K/Si have maxima and successively return to intermediate values throughout the past 10 ka, whereas the Zr/terr and Fe/K show

the same trend as the median grain-size with an increase until 7 ka and a successive decrease.

5. Discussion

5.1. Dilution and dissolution of magnetic minerals

The following discussion focuses on depositional and climatic factors influencing the sediment properties. In contrast to elemental ratios magnetic parameters (ARM_{100 mT}, IRM_{100 mT}) are concentration-dependent. They can be influenced by dilution (marine biogenic contributions) and by post-depositional dissolution (reductive diagenesis). In GeoB9307-3 dilution by biogenic material can be ruled out because Fe/Ca is particularly high when the concentration of magnetic minerals decreases (Fig. 3c, h, i).

Reductive diagenesis will particularly affect fine-grained magnetite (Karlin and Levi, 1983; Canfield and Berner, 1987). Decreasing concentration of fine-grained magnetite (ARM_{100 mT}) is accompanied by decreasing concentration of coarser magnetite (IRM_{100 mT}), the latter being proportionally even stronger. Since the decreasing concentrations do not indicate a preferential depletion of fine grained magnetite, the

reduction of magnetic minerals is unlikely to result from reductive diagenesis. Concentration variations therefore signify variable magnetic mineral proportions in the exported bulk sediments.

5.2. Grain-size and sea-level effects

The grain-size distributions of sediments deposited prior 10.5 ka (Fig. 4c) are bimodal. In the Holocene samples (Fig. 4a, b) the fine fraction is reduced, and even absent in the interval 8.8–5 ka resulting in a unimodal particle-size distribution. The occurrence of fine-grained sediments in surface samples from the shelf of Mozambique was also recognized by Schulz et al. (2011). The authors attributed this fraction to the sediment plume of the Zambezi River deposited on the shelf. The missing fine fraction in the Holocene samples of our record can be explained by two different mechanisms. 1.) Increasing current speeds could initiate winnowing of the sediments. By an extensive mapping approach analyzing time slices of sediment cores retrieved off the Zambezi River, Schulz et al. (2011) found that in times of high sea-level a coast-parallel current developed that deflected the sediment load of the river towards the NE. It could be hypothesized that the initiation of this coast-parallel current is responsible for transporting the fine fraction away from our study site. 2.) Due to the sea-level rise, the distance between river mouth and core location increased. Therefore the sediment plume of the Zambezi River did not reach the core location anymore and the fine fraction was deposited closer to the coast. However, solely based on one sediment core, it is not possible to further constrain the depositional/transport mechanism.

Grain-size variations may affect the geochemical and mineralogical properties of the sediments. Elemental proxies can be influenced by gravitational sorting, since elements as K and Al are enriched in the clay fraction, whereas Si is associated with quartz and feldspars. However, variations in the proxy records are not accompanied by changes in grain size prior to 10.5 ka (Figs. 3, 4c). After 10.5 ka the coarsening (Fig. 3b) is accompanied by an enrichment of heavy minerals (Zr/terr, Fig. 3d), increase in Fe/K (Fig. 3e) and decrease in Al/Si (Fig. 3g). This trend after 10.5 ka can be attributed to gravitational sorting, removing the fine fraction. In the following we will focus on the sediment section deposited before 10.5 ka for which grain-size effects can be neglected.

5.3. Climatic effects

Fig. 5a–c shows three cross plots to evaluate the climatic effects on terrigenous sediment properties. The colors correspond to different time intervals of similar properties. To evaluate the effect of changing precipitation on the proxy records, we plot all parameters against δD ($n\text{-C}_{31}$ alkane) of Schefuß et al. (2011). In monsoonal areas δD of precipitation is negatively correlated to rainfall amounts (Dansgaard, 1964), a signal that is incorporated into plant lipids as long-chained n -alkanes (Schefuß et al., 2005, 2011; Sachse et al., 2012). In contrast, the carbon isotope composition $\delta^{13}\text{C}$ of plant leaf waxes reflects the photosynthetic

pathway of the plants, i.e. the relative contributions of C3 versus C4 plants (e.g., Castaneda et al., 2009). We discuss here only the interval 17–10.5 ka where grain-size effects on the multi-parameter properties are negligible (cf. 5.1). The correlation coefficients shown in Fig. 5 were calculated for this period.

Al represents aluminum silicates (e.g. kaolinite) that form during intensive chemical weathering (e.g., Singer, 1980). The Al/Si therefore serves as a weathering indicator (Govin et al., 2012). A trend of more negative δD (indicating more humid conditions) is related to lower Al/Si (Fig. 5a). Assuming that increasing precipitation would enhance chemical weathering and thus Al/Si would be higher, the expected relation to δD is reversed. Fe/K, which can also serve as a proxy for chemical weathering (Govin et al., 2012), shows no correlation to δD (Fig. 5b). However, it was pointed out that the application of Fe/K as a weathering indicator is biased if the terrigenous fraction contains mafic minerals (Govin et al., 2012). The formation of pedogenic magnetic phases is catalyzed by rainfall (e.g. Maher, 1986; Maher and Thompson, 1992, 1995; Lyons et al., 2010). Therefore, it would be expected that the magnetic mineral content is higher and magnetic inventory is significantly different if soils form under more humid conditions. Similarly as the trend for the major elements, magnetic concentration parameter $\text{IRM}_{100\text{ mT}}$ shows an inverse relation to rainfall (Fig. 5c).

We therefore conclude that the observed variations in elemental ratios and magnetic mineralogy are not due to weathering and/or pedogenic processes catalyzed by rainfall.

5.4. Source area discrimination

We show in Fig. 5d–f selected cross plots of proxies for a more distinct characterization of the terrigenous material deposited during the time span 17–10.5 ka. These cross plots indicate linear relationships between proxies and groups of samples. The concentration of fine grained, SD magnetite (ARM) is correlated with the K/Si ratio, indicating a high depletion of K (leached soil) in the sediments deposited during HS 1 and moderate depletion during the YD (Fig. 5d). The concentration of magnetic and heavy minerals is lowest for HS 1 and YD samples (Fig. 5e). Samples from HS 1 have the lowest S-Ratios and highest $\delta^{13}\text{C}$ n -alkane (data from Schefuß et al., 2011). The levels of the YD samples are moderate and the Bølling–Allerød and Holocene/Pleistocene transition have the highest S-Ratios and lowest $\delta^{13}\text{C}$ (lowest C4 plant contributions, Fig. 5f). These properties will in the following be linked to specific source areas from which terrigenous material was delivered during the past 17 ka.

Beiersdorf et al. (1980) identified three different sedimentary facies on the Mozambique continental shelf and compared their signatures with suspended sediment samples from the Zambezi River and the coastal Cover Sand area (Jaritz et al., 1977). Compared to the Cover Sands, the heavy-mineral concentration in the riverine samples is much higher, representing the hinterland geology (Jaritz et al., 1977). Sediments on the northern shelf correspond to sediments derived

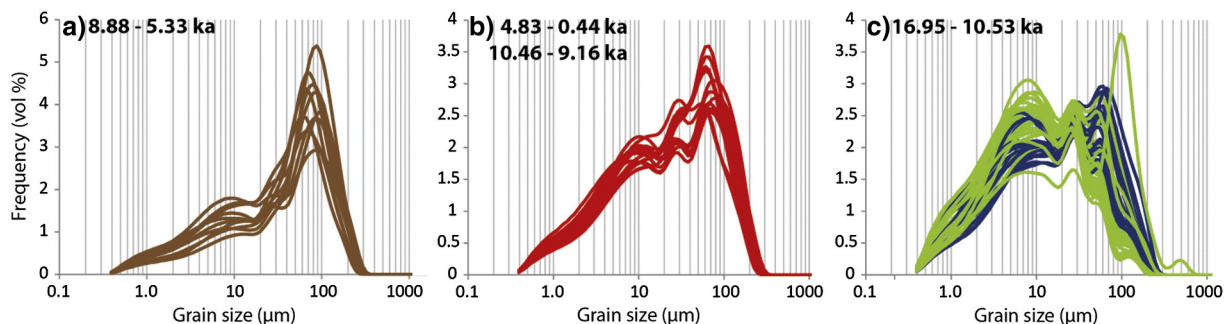


Fig. 4. Grain-size distributions of time intervals. Colors correspond to legend in Fig. 5. (a) Mid-Holocene, (b) Early and Late Holocene, (c) Holocene/Pleistocene transition, YD, Bølling–Allerød, HS 1.

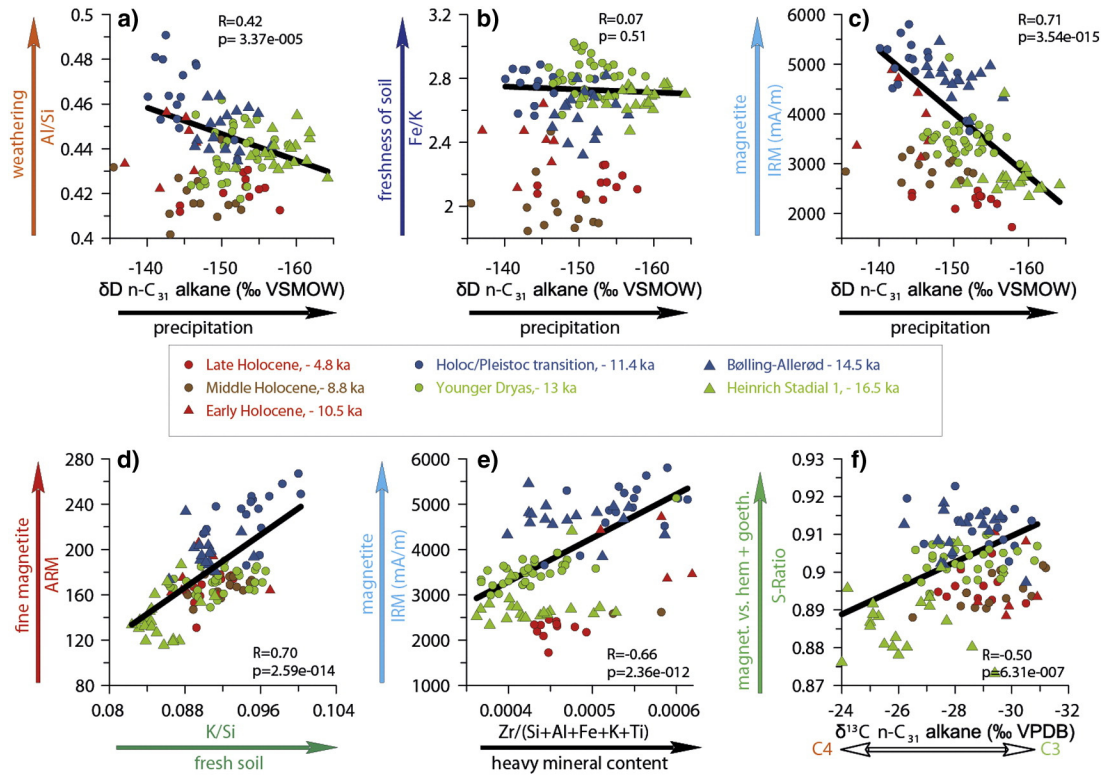


Fig. 5. (a–c) Cross plots evaluating the influence of δD (precipitation proxy, (Schefuß et al., 2011)) on magnetic and elemental properties. (d–e) Cross plots characterizing sediment properties. XRF scanner data (1 cm resolution) were smoothed with a 5 pt running average before interpolating to depth of δD and magnetic properties. The correlation coefficients and p-values were calculated for the sediments deposited prior to 10.5 ka BP, which are not affected by grain-size effects (see text).

from the Cover Sands, while the high-concentrated heavy mineral association off the Zambezi was delivered from the crystalline hinterland (Beiersdorf et al., 1980).

To fingerprint the two different source areas of the sediments in our core, we also consult present-day soil and geologic maps. The coastal area of the Zambezi basin (Cover Sand area) is dominated by siliclastic sediments with patches of silts (Fig. 6a; USGS, 2007). The soils in this area are Fluvisols, Arenosols, Lixisols, and Alisols and have clay contents of 15–30% (FAO et al., 2009). Except in the silt patches, the cation exchange energy is between 50 and 100 cmol kg^{-1} , which is typical for a mixed clay mineralogy, where illite is dominant and kaolinite is depleted (white areas in Fig. 6b; FAO et al., 2009). The hinterland consists of igneous (granites, basalts) and metamorphic (mainly gneisses) basement (Fig. 6a; USGS, 2007). Here the soils have a lower cation exchange energy (Fig. 6b) indicative of kaolinitic soils (FAO et al., 2009).

According to the findings of Beiersdorf et al. (1980) and soil-distribution and lithological maps we propose that sediments with low magnetic mineral concentrations associated with low K/Si and Al/Si and low heavy mineral (Zr) content (time-slices HS 1 and YD, Fig. 5) were derived from the kaolinite-poor Cover Sands in the coastal areas of Mozambique. The high magnetic mineral concentrations occurring with high Al/Si, K/Si and Zr content, on the other hand, likely correspond to material exported from the hinterland with outcrops of igneous basement covered by kaolinitic soils (Fig. 6a, b).

6. Source area activity

6.1. End-member analysis

To further quantify source-area activity and compare it to paleoclimate data we performed end-member (EM) unmixing. In contrast to the elemental ratios that do not always show the same gradual or rapid changes, the magnetic parameters reveal consistent peaks

and trends. We therefore used IRM acquisition curves for the EM approach. The intensity of each EM (Fig. 7a) contribution depends on the concentration of magnetic minerals and on specific magnetic properties of the magnetic minerals contained in the individual sedimentary fractions (Just et al., 2012a,b). Therefore, the intensity can be used to infer the concentration of magnetic minerals within each sedimentary EM and their relative abundance. The IRM acquisition curves are indicative of the magnetic mineral assemblage of each EM (Fig. 7b). A 2 EM model returned reasonable coefficients of determination (0.9–0.99) between input data and estimated IRM acquisition curves for the IRM field steps (Fig. 7c).

The IRM acquisition curve of EM 1 (blue) is shifted towards slightly higher fields and has a somewhat steeper slope in fields higher than 100 mT compared to the curve of EM 2 (red, Fig. 7b). These differences are due to a finer magnetic grain-size of EM 1 and a slightly higher relative proportion of high-coercivity magnetic minerals (goethite and hematite) compared to magnetite.

The downcore mixing coefficients (Fig. 7a) indicate a high contribution of EM 1 (blue) during HS 1 and YD whereas the periods from 14.5 to 13 ka and from 11.4 to 10.5 ka were dominated by EM 2 (red). After 10.5 ka EM 1 re-establishes. The strong increase in total remanent magnetization (SIRM) at the same time when EM 2 proportion increases (15 and 11 ka) and EM 1 is virtually absent (Fig. 7a) indicates that the magnetic mineral concentration in EM 2 is much higher with respect to EM 1. According to Section 5.4 it can be concluded that EM 1 and EM 2 correspond to sediments exported from the heavy mineral depleted Cover Sands and from the hinterland area with a high magnetic mineral content, respectively.

6.2. Climatic controls on sediment export and source area activity

The control mechanisms for the changing source area activity reside in shifting rainfall maxima over East Africa. We shortly outline key

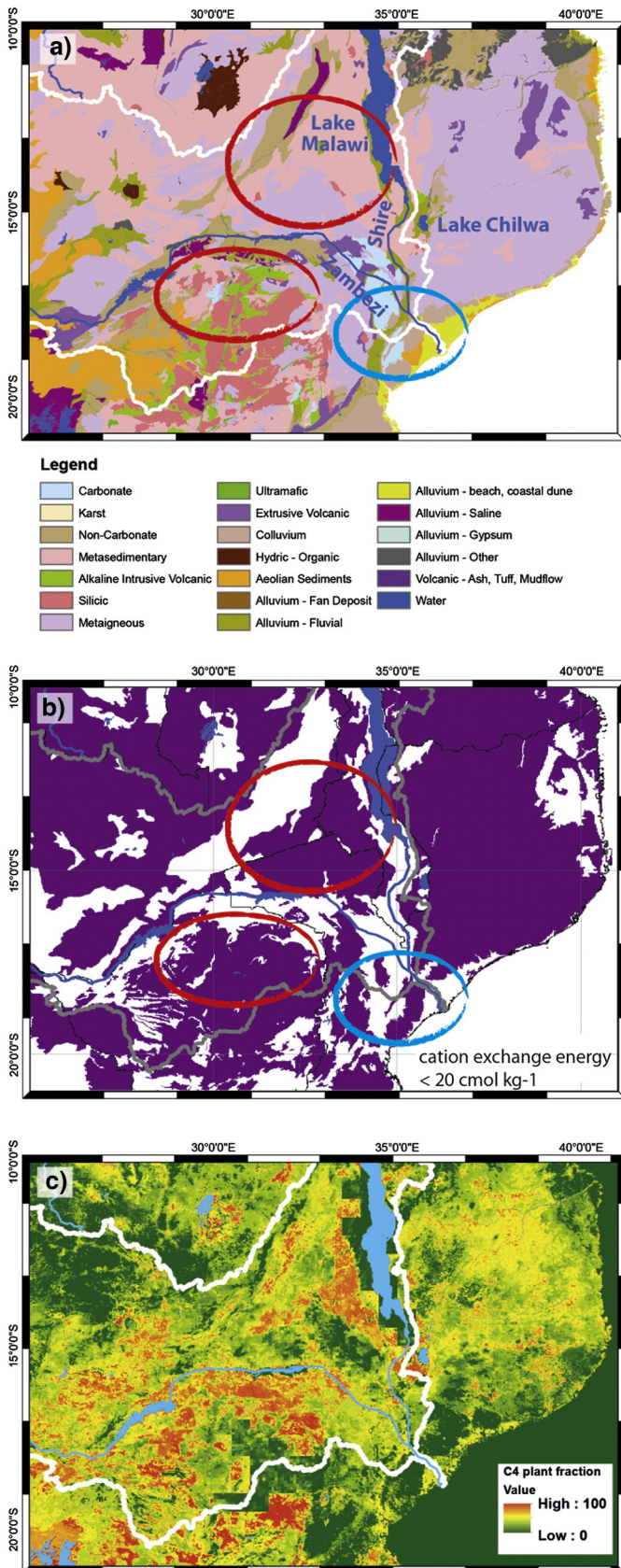


Fig. 6. Maps illustrating (a) lithology (USGS), (b) cation exchange energy $< 20 \text{ cmol kg}^{-1}$, dominated by kaolinite (FAO) and (c) C3/C4 vegetation (Still and Powell, 2010) in the Zambezi Basin. Circles indicate inferred source-areas for HS 1 and YD (blue; EM 1) and Bølling–Allerød and Holocene/Pleistocene transition (red; EM 2). The white lines delineate the Zambezi catchment.

records of changes in hydroclimate. Organic proxies from sites located north of the Zambezi basin as Lake Challa (Tierney et al., 2011) and Lake Tanganyika (Tierney et al., 2008) are characterized by dry conditions during HS 1 and the YD, while at Lake Malawi no change in precipitation was observed (Fig. 8a; Konecky et al., 2011). In contrast, highstand reconstructions from Lake Chilwa (Fig. 8b; Thomas et al., 2009; see Fig. 1 for location) at about 16.2–15.1 ka and 13.5–12.7 ka date to HS 1 and shortly before the YD. The δD record of Geob9307-3 also indicates humid conditions in the Zambezi River basin during HS 1 and the YD (Fig. 8d) (Schefuß et al., 2011). In Lake Tritrivakely (Madagascar) pollen of woody mountain forest increases between 17 and 16 ka, which was interpreted as a humid period after the dry LGM (Gasse and Van Campo, 1998; Gasse, 2000). The shifting rainfall maxima are associated with southward ITCZ displacements during austral summer caused by cold events in the northern high latitudes and leading to higher rainfall in the Zambezi catchment (Schefuß et al., 2011; Wang et al., 2013). A paleoclimatic reconstruction based on pollen distribution in a core retrieved further south off the Limpopo River suggests dry conditions during glaciials and suggests that extension of certain plant taxa was associated to changes in western Indian Ocean SST, being a modulator for summer precipitation south of 20°S (Dupont et al., 2011). Recently, Truc et al. (2013) re-interpreted data from the Wonderkrater (Scott et al., 2003, 2012) and speleothems from the Cold Air Cave (Lee-Thorp et al., 2001; Holmgren et al., 2003) suggesting that HS 1 and the YD were dry in South Africa and precipitation was controlled by Indian Ocean SST. Truc et al. (2013) also re-interpreted the Zambezi record (Schefuß et al., 2011) in the same sense suggesting dry conditions during HS 1 and the YD. This re-interpretation, however, neglects the different moisture-bringing atmospheric systems under the influence of the ITCZ in the Zambezi catchment compared to the region further south and evidence from direct precipitation-related proxy parameters (Schefuß et al., 2011; Wang et al., 2013).

During HS 1 and the YD sediments derived from the coastal regions (EM 1, Fig. 8e) dominate. Fresher material derived from the crystalline basement (EM 2) peaks between HS 1 and YD. The coherent patterns of end-member mixing coefficients and δD (Fig. 8d, e) until 10.5 ka suggest that during times of increased precipitation in the Zambezi basin, material from the proximal siliciclastic deposits was mobilized while the background signal (EM 2) from the hinterland was dominant during drier conditions in the Zambezi basin. After 10.5 ka, the Cover Sand EM 1 gains more importance, still showing a relation to precipitation (δD) but less close. This is probably related to the modified sediment route because of the development of the coast-parallel current (Schulz et al., 2011) (cf., see Section 5.2).

Today, the proximal northern Shire River sub-basin is an important contributor of sediment from the various tributaries of the Zambezi River (Ronco et al., 2006). The Shire's catchment mainly consists of igneous rocks with kaolinite rich soil cover (Fig. 6a, b). Sediments derived from this area will likely contain a high concentration of magnetic minerals and high proportions of weathered clay minerals. These signatures correspond well to our inferred hinterland signatures (cf., see Section 5.4). At times of low precipitation in the Zambezi catchment sediment export by the Shire, draining the northernmost Zambezi Basin, that at present receives more rain than the central basin (Ronco et al., 2006), could thus have caused higher relative contribution of the hinterland EM.

At present, the hinterland of the Zambezi Basin, including the Shire River sub-basin, is dominated by C4 plants while C3 plants have a higher relative abundance in the gross of the Cover Sand area (Fig. 6c). The $\delta^{13}\text{C}$ isotopic compositions of plant waxes (Schefuß et al., 2011) indicate higher contributions from C4 plants during HS 1 and YD (Figs. 5f, 8c) which was interpreted as a source-area shift of organic material from the coastal area (C3 vegetation) to the lower Zambezi floodplain (C4 vegetation) (Schefuß et al., 2011). From a sedimentological perspective this shift is not evident because the lithologies in these areas are similar and a shift from hinterland (EM 2) to Cover Sands (EM 1) is detected for

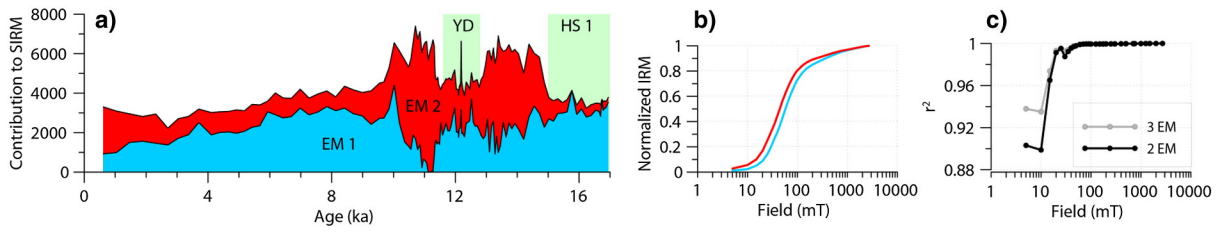


Fig. 7. End-member unmixing of IRM acquisition curves. (a) Contribution to SIRM of unmixed EMs. EM 1 (blue): Cover Sand EM, EM 2 (red): hinterland EM, see also Fig. 6. (b) IRM acquisition curves for EMs in (a). (c) Coefficient of determination for individual IRM steps of a 2 and 3 EM mixing model.

times of higher precipitation. This discrepancy might be attributed to a de-coupling of the terrigenous sedimentary and plant organic signals. We propose that at times of low precipitation and low Zambezi discharge, sediments were mainly derived from the hinterland (EM 2) and transported through the Zambezi system. The initial, relatively low content of C4-derived plant material could have been effectively overprinted by the addition of C3 plant organic contributions in the lower Zambezi reaches whereas the sedimentological signal remained unaltered. In contrast, at times of high precipitation in the Zambezi catchment and high discharge, the initial river-transported sedimentological hinterland signal (EM 2) could have been overprinted by the Cover Sand EM 1. The high content of C4 plant-derived organic material was not sufficiently diluted because of the sparse C3-vegetation cover in the Cover Sand area. Such a process would effectively explain the apparent de-coupling of sedimentological and organic signals with variable Zambezi discharge.

7. Conclusions

Many multiproxy studies utilize organic, granulometric, geochemical and magnetic data to characterize changes in terrigenous sediment

accumulation in the ocean and to draw conclusions about environmental conditions on land. However, variations in the proxy records of GeoB9307-3 and equivalent end-member mixing coefficients rather represent changes in the source area activity within the Zambezi River basin than being a representation of climate induced weathering processes in the entire basin. Nonetheless, the source-area activity is controlled by climatic conditions. Periods of increased rainfall in the Zambezi basin associated to southward ITCZ shifts initiated sediment mobilization from loosely vegetated coastal regions, while the background signal from hinterland soils was diluted. This terrigenous fraction has low heavy and magnetic mineral concentrations and low Al/Si and K/Si ratios. High magnetic mineral concentrations in the sediment core off the Zambezi and high K/Si and Al/Si ratios correspond to relatively increased sedimentary contributions from the northern sub-basin. A de-coupling of sedimentary and organic signals is evident and might be explained by overprinting of the sedimentary signal by high erosional activity at high discharge and by the addition of plant material to the organic signals at times of low discharge. We propose that a careful consideration of changes of source areas is needed when reconstructing terrestrial climate conditions from marine sedimentary archives.

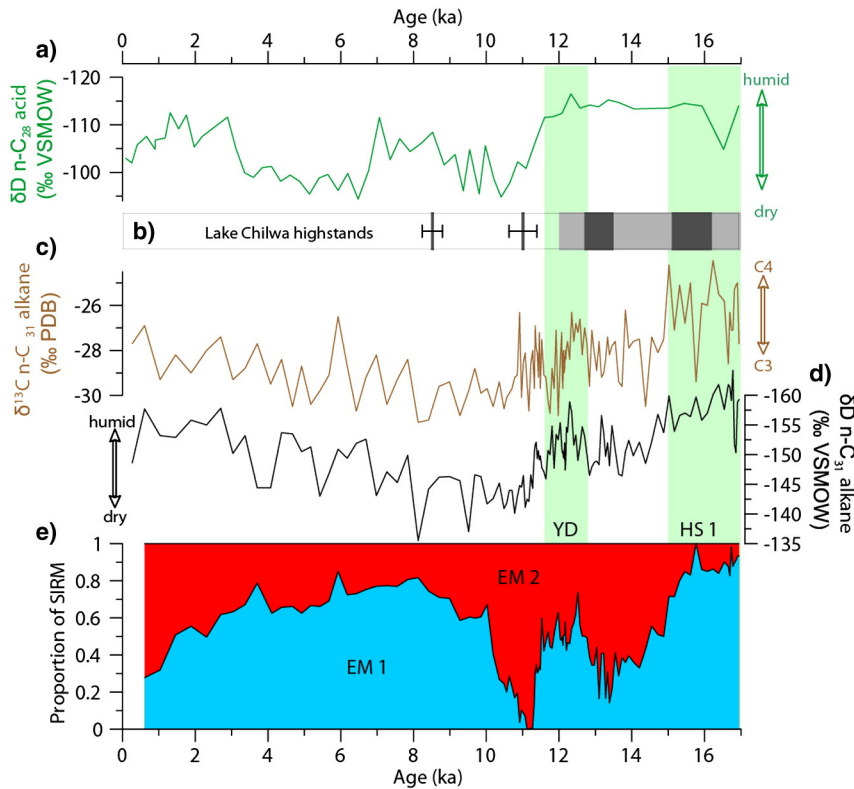


Fig. 8. Climatic conditions inducing source area activity. (a) $\delta^{13}\text{D}$ of *n*-acids from Lake Malawi (Konecny et al., 2011). (b) Highstands in Lake Chilwa dated by total error method (gray bars) and Finite Mixture Model (black bars) (Thomas et al., 2009). (c) $\delta^{13}\text{C}$ of *n*-alkanes of GeoB9307-3 (Scheffuß et al., 2011) (d) δD of *n*-alkanes of GeoB9307-3 (Scheffuß et al., 2011). (e) Normalized end-member contributions shown in Fig. 7a.

Acknowledgments

This research used data acquired at the XRF Core Scanner Lab at the MARUM, Center for Marine Environmental Sciences and magnetic measurements in the Marine Geophysics Group, University of Bremen, Germany. We thank M. Zabel for EDP XRF analyses and the crew and scientific party of M63/1. We thank two anonymous reviewers for constructive suggestions. This study was funded through DFG–Research Center/Cluster of Excellence “The Ocean in the Earth System”. Data used in this publication can be found <http://doi.pangaea.de/10.1594/PANGAEA.830066>.

References

- Beiersdorf, H., Kudrass, H.-R., von Stackelberg, U., 1980. Placer deposits of ilmenite and zircon on the Zambezi Shelf. *Geol. Jahrb.* 36.
- Biscaye, P.E., 1965. Mineralogy and sedimentation of recent deep-sea clay in the Atlantic Ocean and adjacent seas and oceans. *Geol. Soc. Am. Bull.* 76, 803–832.
- Blanchet, C.L., Tjallingii, R., Frank, M., Lorenzen, J., Reitz, A., Brown, K., Feseker, T., Brückmann, W., 2013. High- and low-latitude forcing of the Nile River regime during the Holocene inferred from laminated sediments of the Nile deep-sea fan. *Earth Planet. Sci. Lett.* 364, 98–110.
- Bloemendal, J., King, J.W., Hall, F.R., Doh, S.J., 1992. Rock magnetism of Late Neogene and Pleistocene deep-sea sediments: relationship to sediment source, diagenetic processes, and sediment lithology. *J. Geophys. Res.* 97, 4361–4375.
- Bloemsma, M.R., Zabel, M., Stuut, J.B.W., Tjallingii, R., Collins, J.A., Weltje, G.J., 2012. Modelling the joint variability of grain size and chemical composition in sediments. *Sediment. Geol.* 280, 135–148.
- Boyle, E.A., 1983. Chemical accumulation variations under the Peru current during the past 130,000 years. *J. Geophys. Res.* 88, 7667–7680.
- Camoin, G.F., Montaggioni, L.F., Braithwaite, C.J.R., 2004. Late glacial to post glacial sea levels in the Western Indian Ocean. *Mar. Geol.* 206, 119–146.
- Canfield, D.E., Berner, R.A., 1987. Dissolution and pyritization of magnetite in anoxic marine sediments. *Geochim. Cosmochim. Acta* 51, 645–659.
- Caqueneau, S., Gaudichet, A., Gomes, L., Legrand, M., 2002. Mineralogy of Saharan dust transported over northwestern tropical Atlantic Ocean in relation to source regions. *J. Geophys. Res.* 107, 4251.
- Castañeda, I., Mulitza, S., Schefuß, E., Lopes dos Santos, R., Sinninghe Damsté, J., Schouten, S., 2009. Wet phases in the Sahara/Sahel region and human migration patterns in North Africa. *Proc. Natl. Acad. Sci. U. S. A.* 106, 20159–20163.
- Clark, D., Emerson, D., 1991. Notes on rock magnetization characteristics in applied geophysical studies. *Explor. Geophys.* 22, 547–555.
- Dansgaard, W., 1964. Stable isotopes in precipitation. *Tellus* 16, 436–468.
- deMenocal, P.B., Bloemendal, J., King, J., et al., 2001. A rock-magnetic record of monsoonal dust deposition to the Arabian sea: evidence for a shift in the mode of deposition at 2.4 Ma. In: *Prell, W.L., Niitsuma, N. (Eds.), Proc. ODP, Sci. Results. College Station, Texas*, pp. 389–407.
- Dupont, L.M., Caley, T., Kim, J.H., Castañeda, I., Malaizé, B., Giraudeau, J., 2011. Glacial–interglacial vegetation dynamics in South Eastern Africa coupled to sea surface temperature variations in the Western Indian Ocean. *Clim. Past* 7, 1209–1224.
- Eyre, J., 1996. The application of high resolution IRM acquisition to the discrimination of remanence carriers in Chinese loess. *Stud. Geophys. Geod.* 40, 234–242.
- FAO, IIASA, ISRIC, ISSCAS, JRC, IIASA, 2009. Harmonized World Soil Database (version 1.1). In: *FAO, IIASA (Eds.), (Rome, Italy and Laxenburg, Austria)*.
- Fitzpatrick, R.W., Schwertmann, U., 1982. Al-substituted goethite—an indicator of pedogenic and other weathering environments in South Africa. *Geoderma* 27, 335–347.
- Frank, U., Nowaczyk, N.R., 2008. Mineral magnetic properties of artificial samples systematically mixed from haematite and magnetite. *Geophys. J. Int.* 175, 449–461.
- Frederichs, T., Bleil, U., Däumler, K., von Döbenek, T., Schmidt, A., 1999. The magnetic view on the marine paleoenvironment: parameters, techniques and potentials of rock magnetic studies as a key to paleoclimatic and paleoceanographic changes. In: *Fischer, G., Wefer, G. (Eds.), Use of Proxies in Paleoceanography: Examples from the South Atlantic*. Springer, Berlin, Heidelberg.
- Gasse, F., 2000. Hydrological changes in the African tropics since the Last Glacial Maximum. *Quat. Sci. Rev.* 19, 189–211.
- Gasse, F., Van Campo, E., 1998. A 40,000-yr pollen and diatom record from Lake Tritrivakely, Madagascar, in the southern tropics. *Quat. Res.* 49, 299–311.
- Govin, A., Holzwarth, U., Heslop, D., Ford Keeling, L., Zabel, M., Mulitza, S., Collins, J.A., Chiessi, C.M., 2012. Distribution of major elements in Atlantic surface sediments (36°N–49°S): imprint of terrigenous input and continental weathering. *Geochim. Geophys. Geosyst.* 13, Q01013.
- Hanesch, M., Scholger, R., 2005. The influence of soil type on the magnetic susceptibility measured throughout soil profiles. *Geophys. J. Int.* 161, 50–56.
- Heslop, D., Dillon, M., 2007. Unmixing magnetic remanence curves without *a priori* knowledge. *Geophys. J. Int.* 170, 556–566.
- Heslop, D., von Döbenek, T., Höcker, M., 2007. Using non-negative matrix factorization in the “unmixing” of diffuse reflectance spectra. *Mar. Geol.* 241, 63–78.
- Holmgren, K., Lee-Thorp, J.A., Cooper, G.R.J., Lundblad, K., Partridge, T.C., Scott, L., Sthaldean, R., Siep Talma, A., Tyson, P.D., 2003. Persistent millennial-scale climatic variability over the past 25,000 years in Southern Africa. *Quat. Sci. Rev.* 22, 2311–2326.
- Jaritz, W., Ruder, J., Schlenker, B., 1977. Das Quartär im Küstengebiet von Moçambique und seine Schwermineralführung. *Geol. Jahrb.* 26.
- Just, J., Dekkers, M.J., von Döbenek, T., van Hoesel, A., Bickert, T., 2012a. Signatures and significance of aeolian, fluvial, bacterial and diagenetic magnetic mineral fractions in Late Quaternary marine sediments off Gambia, NW Africa. *Geochim. Geophys. Geosyst.* 13, Q0A002.
- Just, J., Heslop, D., von Döbenek, T., Bickert, T., Dekkers, M.J., Frederichs, T., Meyer, I., Zabel, M., 2012b. Multiproxy characterization and budgeting of terrigenous end-members at the NW African continental margin. *Geochim. Geophys. Geosyst.* 13, Q0A001.
- Kämpf, N., Schwertmann, U., 1983. Goethite and hematite in a climosequence in southern Brazil and their application in classification of kaolinitic soils. *Geoderma* 29, 27–39.
- Karlin, R., Levi, S., 1983. Diagenesis of magnetic minerals in recent haemipelagic sediments. *Nature* 303, 327–330.
- King, J., Banerjee, S.K., Marvin, J., Özdemir, Ö., 1982. A comparison of different magnetic methods for determining the relative grain size of magnetite in natural materials: some results from lake sediments. *Earth Planet. Sci. Lett.* 59, 404–419.
- Köhler, C.M., Heslop, D., Dekkers, M.J., Krijgsman, W., van Hinsbergen, D.J.J., von Döbenek, T., 2008. Tracking provenance change during the late Miocene in the eastern Mediterranean using geochemical and environmental magnetic parameters. *Geochim. Geophys. Geosyst.* 9.
- Konecky, B.L., Russell, J.M., Johnson, T.C., Brown, E.T., Berke, M.A., Werne, J.P., Huang, Y., 2011. Atmospheric circulation patterns during late Pleistocene climate changes at Lake Malawi, Africa. *Earth Planet. Sci. Lett.* 312, 318–326.
- Kruijver, P.P., Passier, H., 2001. Coercivity analysis of magnetic phases in sapropel S1 related to variations in redox conditions, including an investigation of the S ratio. *Geochim. Geophys. Geosyst.* (2).
- Larrasoña, J.C., Roberts, A.P., Rohling, E.J., 2008. Magnetic susceptibility of eastern Mediterranean marine sediments as a proxy for Saharan dust supply? *Mar. Geol.* 254, 224–229.
- Lee-Thorp, J.A., Holmgren, K., Lauritzen, S.E., Linge, H., Moberg, A., Partridge, T.C., Stevenson, C., Tyson, P.D., 2001. Rapid climate shifts in the southern African interior throughout the Mid to Late Holocene. *Geophys. Res. Lett.* 28, 4507–4510.
- Lyons, R., Oldfield, F., Williams, E., 2010. Mineral magnetic properties of surface soils and sands across four North Africa transects and links to climatic gradients. *Geochim. Geophys. Geosyst.* 11, Q08023.
- Lyons, R., Oldfield, F., Williams, E., 2012. The possible role of magnetic measurements in the discrimination of Sahara/Sahel dust sources. *Earth Surf. Process. Landf.* 37, 594–606.
- Maher, B.A., 1986. Characterisation of soils by mineral magnetic measurements. *Phys. Earth Planet. Inter.* 42, 76–92.
- Maher, B.A., Taylor, R.M., 1988. Formation of ultrafine-grained magnetite in soils. *Nature* 336, 368–370.
- Maher, B.A., Thompson, R., 1992. Paleoclimatic significance of the mineral magnetic record of the Chinese loess and paleosols. *Quat. Res.* 37, 155–170.
- Maher, B.A., Thompson, R., 1995. Paleorainfall reconstructions from pedogenic magnetic susceptibility variations in the Chinese Loess and paleosols. *Quat. Res.* 44, 383–391.
- Maher, B.A., Watkins, S.J., Brunskill, G., Alexander, J., Fielding, C.R., 2009. Sediment provenance in a tropical fluvial and marine context by magnetic ‘fingerprinting’ of transportable sand fractions. *Sedimentology* 56, 841–861.
- Mathias, G.L., Nagai, R.H., Trindade, R.I.F., de Mahiques, M.M., 2014. Magnetic fingerprint of the late Holocene inception of the Rio de la Plata plume onto the southeast Brazilian shelf. *Palaeogeogr. Palaeoclimatol. Palaeoecol.* <http://dx.doi.org/10.1016/j.palaeo.2014.03.034> (in press).
- Meade, R.H., 1994. Suspended sediments of the modern Amazon and Orinoco rivers. *Quat. Int.* 21, 29–39.
- Meyer, I., Davies, G.R., Vogt, C., Kuhlmann, H., Stuut, J.-B.W., 2013. Changing rainfall patterns in NW Africa since the Younger Dryas. *Aeolian Res.* 10, 111–123.
- Mulitza, S., Prange, M., Stuut, J.B., Zabel, M., von Döbenek, T., Itambi, A.C., Nizou, J., Schulz, M., Wefer, G., 2008. Sahel megadroughts triggered by glacial slowdowns of Atlantic meridional overturning. *Paleoceanography* 23, PA4206.
- Oldfield, F., Rummery, T.A., Thompson, R., Walling, D.E., 1979. Identification of suspended sediment sources by means of magnetic measurements: some preliminary results. *Water Resour. Res.* 15, 211–218.
- Ronco, P., Fasolato, G., Di Silvio, G., 2006. The case of the Zambezi River in Mozambique: some investigations on solid transport phenomena downstream Cahora Bassa Dam. In: *Alves, E., Cardoso, A., Leal, J., Ferreira, R. (Eds.), Proc. Int. Confer. Fluvial Hydraul. Taylor & Francis, Lisbon, Portugal*.
- Sachse, D., Billault, I., Bowen, G.J., Chikaraishi, Y., Dawson, T.E., Feakins, S.J., Freeman, K.H., Magill, C.R., McInerney, F.A., van der Meer, M.T.J., Polissar, P., Robins, R.J., Sachs, J.P., Schmidt, H.-L., Sessions, A.L., White, J.W.C., West, J.B., Kahmen, A., 2012. Molecular paleohydrology: interpreting the hydrogen-isotopic composition of lipid biomarkers from photosynthesizing organisms. *Ann. Rev. Earth Planet. Sci.* 40, 221–249.
- Schefuß, E., Schouten, S., Schneider, R.R., 2005. Climatic controls on central African hydrology during the past 20,000 years. *Nature* 437, 1003–1006.
- Schefuß, E., Kuhlmann, H., Mollenhauer, G., Prange, M., Patzold, J., 2011. Forcing of wet phases in southeast Africa over the past 17,000 years. *Nature* 480, 509–512.
- Schmidt, A.M., von Döbenek, T., Bleil, U., 1999. Magnetic characterization of Holocene sedimentation in the South Atlantic. *Paleoceanography* 14, 465–481.
- Schneider, R.R., Price, B., Müller, P.J., Kroon, D., Alexander, I., 1997. Monsoon related variations in Zaire (Congo) sediment load and influence of fluvial siliciclastic supply on marine productivity in the east equatorial Atlantic during the last 200,000 years. *Paleoceanography* 12, 463–481.
- Schulz, H., Lückge, A., Emeis, K.-C., Mackensen, A., 2011. Variability of Holocene to Late Pleistocene Zambezi riverine sedimentation at the upper continental slope off Mozambique, 15°–21°S. *Mar. Geol.* 286, 21–34.

- Schwertmann, U., Taylor, R.M., 1989. Iron Oxides. Soil Science Society of America Inc. (SSSA), Madison, USA.
- Scott, L., Holmgren, K., Talma, A.S., Woodborne, S., Vogel, J.C., 2003. Age interpretation of the Wonderkrater spring sediments and vegetation change in the Savanna Biome, Limpopo province, South Africa. *S. Afr. J. Sci.* 99.
- Scott, L., Neumann, F.H., Brook, G.A., Bousman, C.B., Norström, E., Metwally, A.A., 2012. Terrestrial fossil-pollen evidence of climate change during the last 26 thousand years in Southern Africa. *Quat. Sci. Rev.* 32, 100–118.
- Singer, A., 1980. The paleoclimatic interpretation of clay minerals in soils and weathering profiles. *Earth Sci. Rev.* 15, 303–326.
- Singer, A., 1984. The paleoclimatic interpretation of clay minerals in sediments — a review. *Earth Sci. Rev.* 21, 251–293.
- Still, C., Powell, R., 2010. Continental-Scale Distributions of Vegetation Stable Carbon Isotope Ratios. In: Bowen, G.J., Dawson, T.E., Tu, K.P., West, J.B. (Eds.), *Isoscapes*. Springer, Netherlands, pp. 179–193.
- Thomas, D.S.G., Bailey, R., Shaw, P.A., Durcan, J.A., Singarayer, J.S., 2009. Late Quaternary highstands at Lake Chilwa, Malawi: frequency, timing and possible forcing mechanisms in the last 44 ka. *Quat. Sci. Rev.* 28, 526–539.
- Tierney, J.E., Russell, J.M., Huang, Y., Damsté, J.S.S., Hopmans, E.C., Cohen, A.S., 2008. Northern hemisphere controls on tropical southeast African climate during the past 60,000 years. *Science* 322, 252–255.
- Tierney, J.E., Russell, J.M., Sinninghe Damsté, J.S., Huang, Y., Verschuren, D., 2011. Late Quaternary behavior of the East African monsoon and the importance of the Congo Air Boundary. *Quat. Sci. Rev.* 30, 798–807.
- Truc, L., Chevalier, M., Favier, C., Cheddadi, R., Meadows, M.E., Scott, L., Carr, A.S., Smith, G.F., Chase, B.M., 2013. Quantification of climate change for the last 20,000 years from Wonderkrater, South Africa: implications for the long-term dynamics of the Intertropical Convergence Zone. *Palaeogeogr. Palaeoclimatol. Palaeoecol.* 375–387.
- Türkay, M., Pätzold, J., 2009. Southwestern Indian Ocean — Eastern Atlantic Ocean, Cruise No 63, January 24–March 30, 2005, METEOR-Berichte. Universität Hamburg, p. 98.
- USGS, 2007. Global Ecosystems.
- Wang, Y.V., Larsen, T., Leduc, G., Andersen, N., Blanz, T., Schneider, R.R., 2013. What does leaf wax δD from a mixed C3/C4 vegetation region tell us? *Geochim. Cosmochim. Acta* 11, 128–139.
- Weltje, G., 1997. End-member modeling of compositional data: numerical-statistical algorithms for solving the explicit mixing problem. *Math. Geol.* 29, 503–549.
- Weltje, G.J., Tjallingii, R., 2008. Calibration of XRF core scanners for quantitative geochemical logging of sediment cores: theory and application. *Earth Planet. Sci. Lett.* 274, 423–438.
- Wien, K., Wissmann, D., Kölling, M., Schulz, H.D., 2005. Fast application of X-ray fluorescence spectrometry aboard ship: how good is the new portable Spectro Xepos analyser? *Geo-Mar. Lett.* 25, 248–264.
- Williams, M., Talbot, M., Aharon, P., Abdl Salaam, Y., Williams, F., Inge Brendeland, K., 2006. Abrupt return of the summer monsoon 15,000 years ago: new supporting evidence from the lower White Nile valley and Lake Albert. *Quat. Sci. Rev.* 25, 2651–2665.
- Zabel, M., Schneider, R.R., Wagner, T., Adegbe, A.T., de Vries, U., Kolonic, S., 2001. Late Quaternary climate changes in Central Africa as inferred from terrigenous input to the Niger Fan. *Quat. Res.* 56, 207–217.
- Zambezi Watercourse Commission, 2008. Integrated Water Resources Management Strategy and Implementation Plan for the Zambezi River Basin.